AMERICAN SCIENTIFIC PUBLISHERS

Advanced Science, Engineering and Medicine
Vol. 5, pp. 1–7, 2013
(www.aspbs.com/asem)

ARTICLE

Synthesis and Characterization of Europium-Doped Zinc Sulphide (ZnS:Eu) Nano Particles: Nano Red Phosphor

I. Ahemen[1,*] and Dilip K. De[2]

[1]*Department of Physics, University of Agriculture Makurdi, Nigeria*
[2]*Department of Physics, University of Jos, Plateau State, Nigeria*

A preliminary work on synthesis of Europium-doped Zinc sulphide nanophosphors is reported. The result shows that pure and well passivated ZnS:Eu^{3+} nano-particles were synthesized. The average particle sizes show that the nano-particles are in the strong quantum confinement regime which is evident from the stoke-shift in the absorption spectrum and the broadening of the XRD diffraction peaks. Particles sizes determined from the effective mass approximation and hyperbolic band model show higher particle size distribution, as a result of a consequential failure of these models at very small size regime. The intensity of red light emitted from the synthesized ZnS:Eu nanophospors is size and site dependent. There is clear evidence that energy transfer from ZnS host to Eu^{3+} occurred but this emission has weak intensity.

KEYWORDS: Synthesis, Characterization, Europium, Zinc Sulphide, Nano Red Phosphor, Energy Transfer, Confinement and Red Light, Particle Size.

1. INTRODUCTION

The energy inefficiency and environmental consequences[1] of conventional lighting sources such as incandescent and fluorescent lamps has led to a new lighting technology known as solid state lighting (SSL) using light emitting diodes (LEDs). It is expected that LEDs emitting white light would find wide-ranging applications as lighting sources and save huge energy world-wide. LED is mainly a *p–n* junction injected device, adopting semiconductor materials (like InGaN) to generate light through electron–hole pair recombination.[2] The energy of emitted photon is approximately equivalent to the energy difference of the semiconductor bandwidth. Therefore, the emission is a narrow band and so appears to be colored. For most of the household, educational and industrial works white light sources are preferred to colored light sources. To obtain broad-band light (i.e., white light), two approaches are considered—the color mixing approach and the phosphor down-conversion method.[3]

The color mixing approach involves mixing a blue LED, green LED and red LED to obtain white light. This technique produces white light with superior color rendering index (CRI), low correlate color temperature (CCT), and high efficiency.[3] The disadvantages of this approach are the complexity of the drive and control circuitry and the differences in temperature variations among LEDs.[4] The phosphor-down conversion method is subdivided into two—the first is using a blue InGaN LED to excite a yellow (YAG:Ce) phosphor to generate white light with low CRI, high CCT and low conversion efficiency. Despite the low energy efficiency this is the most commercialized method of white LED even though the white light generated is highly deficient in the red spectrum. The second down conversion method involves pumping a combination of green, yellow and red phosphor with near-ultraviolet (UV) LED to generate white light. The white light obtained under this technique has high CRI, low CCT and high energy efficiency.[5]

In recent time scientists have focused attention towards finding good complementary red-light emitting phosphors[5] and Eu-doped ZnS nano-phosphor is a potential candidate. ZnS is a direct band gap semiconductor with energy gap (∼3.6 eV) wide enough to be transparent to the whole visible spectrum. ZnS has two crystal structures; the zincblende and the hexagonal crystal structures when processed at low and high temperatures respectively (Shepherd and Holloway (2004)).[6] The wide band gap of ZnS and the ability to vary this band gap with reduced particle size (at nanoscale) makes this semiconductor to be a good host matrix.[7]

*Author to whom correspondence should be addressed.
Email:
Received: 8 February 2013
Accepted: 22 April 2013

ARTICLE

Europium (Eu^{3+} ion) is a good luminescent center for red light emission.[8] The transitions in Eu^{3+} are however localized to the $4f^n$ shell because of the shielding effect of the 5s and 5p shell electrons.[9] Thus, the energy of the corresponding levels of $4f^n$ configuration is weakly sensitive to the type of crystal host and is treated as free-ion state.[10] Consequently, direct excitation of Eu^{3+} ion is unfavorable because of weak absorbance.[11] This problem may be resolved by coupling species (host matrices) that are able to participate in energy transfer processes.[12] Though, optical transitions in Eu^{3+} ion is forbidden by selection rules the lack of center of symmetry or inversion on the tetrahedron site of Zn^{2+} ion relaxes the parity selection rules for the $f-f$ intra-band transitions inherent in Eu^{3+} ion when this ion is substituted into Zinc lattice site. This occurs because of the mixing of electronic states of different parities.[13]

To explore the possibility of generating white light with high CRI, low CCT and high efficiency using LEDs, this work is focused on the synthesis and characterization of Eu-doped ZnS nanoparticle that could serve as a potential candidate for red-emitting phosphor.

2. EXPERIMENTAL DETAILS

Eu^{3+}-doped ZnS was synthesized by a chemical precipitation method using $Zn(CHCOO)_2 \cdot 2H_2O$ (Kermel), $EuCl_3$ (Sigma-Aldrich) and $Na_2S \cdot 9H_2O$ (Sigma-Aldrich) as starting materials. First, $Zn(CHCOO)_2 \cdot 2H_2O$ and $EuCl_3$ were dissolved in a mix medium of deionized water and methanol. The concentration of Eu^{3+} ion was set at 1%, 2% and 5% in molar ratio of Eu^{3+} ion to Zn^{2+} ion. α-Methacrylic acid (MA) was also added to the reaction medium as a capping agent. Then, water-methanol binary solution of $Na_2S \cdot 9H_2O$ was added drop-wise into the above mixture along with continuous stirring. The formed nanoparticles were centrifugally separated from the solution. After repeated washing with deionized water and menthanol and then dried under vacuum for 2 hours at 90 °C, the powder sample of ZnS nanoparticle doped with Eu^{3+} ion was obtained. The samples are named ZE1, ZE2 and ZE5 for 1%, 2% and 5% molar ratio of Eu^{3+} doping concentrations respectively. The samples were then characterized using Scanning Electron microscopy, Fourier Transform Infrared spectroscopy, X-ray Diffraction, UV-Visible spectroscopy, and Photoluminescence studies.

3. RESULTS AND DISCUSSION

3.1. UV-Visible Spectroscopy

The UV-Visible absorption spectra of Eu^{3+}-doped ZnS nanoparticles (ZE1, ZE2 and ZE5) are shown in Figure 1. The following Tauc's relation was used to determine the energy band gap of the nanoparticles[14] (http://cnx.org/content/m43554/latest/):

$$\omega^2 \varepsilon = A(h\nu - E_g)^n \tag{1}$$

where, ε is optical absorbance, E_g is the band gap of the material, $\omega = 2\pi c/\lambda = 2\pi v$ is the angular frequency of the incident radiation (λ is the gap wavelength) and exponent n depends on the type of transition.

Here, the transition is direct so we have $n = 1/2$. The bandgap wavelength can be obtained by extrapolating the straight line portion of ε^2/λ versus $1/\lambda$ graph to intersect the $1/\lambda$ axis (Fig. 1(b)). The bandgap wavelengths are 309 nm, 309 nm and 305 nm for ZE1, ZE2 and ZE5 respectively (Fig. 1(b)). Therefore, using the above bandgap wavelengths, the optical band gap energy (E_g) was calculated based on:

$$E_g = hc/\lambda \tag{2}$$

Where h is Planck's constant, c is the speed of light in vacuum and λ is the bandgap wavelength.

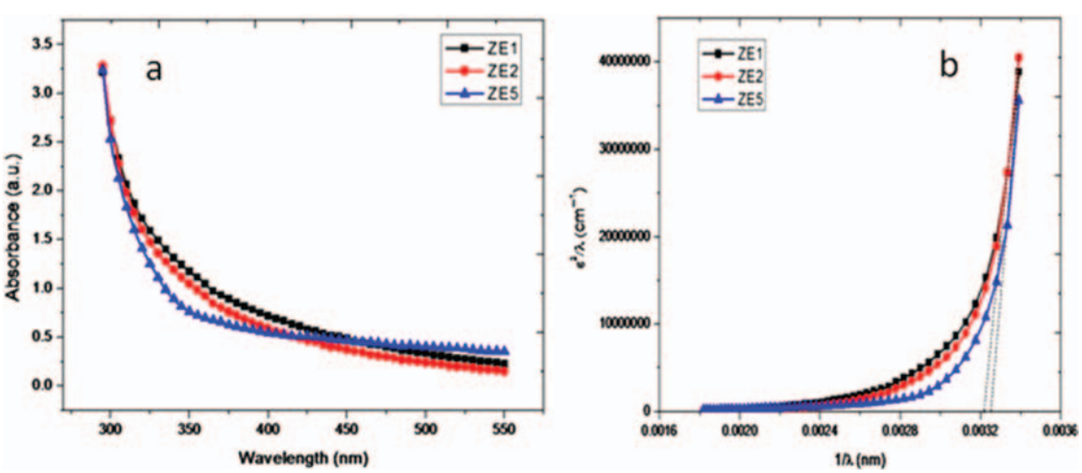

Fig. 1. Optical absorption spectra (a) absorbance Spectra and (b) ε^2/λ versus $1/\lambda$ spectra for ZE1, ZE2 and ZE5 samples.

Table I. Energy and average particles size distribution in ZE1, ZE2 and ZE5 samples.

Sample type	Energy Bandgap (eV)	Stoke's shift (eV)	Particles/crystallite size (nm)			
			TEM	XRD	EMA	HBM
ZE1	4.02 (309 nm)	0.42	–	1.95	4.38	4.12
ZE2	4.02 (309 nm)	0.42	4.11	2.14	4.38	4.12
ZE5	4.07 (305 nm)	0.47	–	2.71	4.18	3.88

The obtained bandgap energies of the different samples are shown in Table I. The energy bandgaps show blue shift of 0.42–0.47 eV of the absorption band from the bulk value of 3.60 eV for the zinc blende (ZnS) crystal at room temperature.

Using the values of the calculated bandgap energies, the particles sizes of all the samples were calculated using the effective mass approximation (EMA) as given[15, 16] by Eq. (3).

$$E_n = E_b + \frac{\hbar^2\pi^2}{2r^2}\left(\frac{1}{m_e^*}+\frac{1}{m_h^*}\right) - \frac{1.8e^2}{4\pi\varepsilon\varepsilon_0 r} - \frac{0.124e^4}{\hbar^2(4\pi\varepsilon\varepsilon_0)^2}\left(\frac{1}{m_e^*}+\frac{1}{m_h^*}\right)^{-1} \quad (3)$$

Also, the hyperbolic band model (HBM) was used to determine their particle sizes. HBM is modification of EMA and it accounts for the approximation to hyperbolic band (Eq. (4)) in the small size regime (< 10 nm):[17]

$$(\hbar\omega)^2 = \left(\frac{hc}{\lambda}\right)^2 = \left(\frac{2\hbar^2 E_g}{m^*}\right)\left(\frac{\pi}{r}\right)^2 + E_g^2 \quad (4)$$

where r is nanoparticles size, E_b is the bandgap energy of bulk ZnS, E_g is the energy of the nanocrystal, e is the electron charge, ε is dielectric constant of ZnS, ε_0 is the permittivity of free space, m_e^* and m_h^* are the effective electron and holes masses respectively.

The values of the particle sizes are comparable to the exciton Bohr radius ($\alpha_1 B = 2.6$ nm) for ZnS, supporting the quantum confinement effect. The higher values of the particle size obtained using EMA is as a result of the quantitative failure of the EMA in explaining the result for very small particles (< 5 nm).[18] The failure of EMA is also because the values of the effective masses used are those of bulk ZnS. The assumption of parabolic energy bands and the non-spherical geometry of the nanoparticles could also have caused a quantitative failure[19] of the EMA.

3.2. Photoluminescence Studies

Photoluminescence excitation (PLE) spectrum obtained by monitoring the $^5D_0 \rightarrow {}^7F_2$ transition (618 nm) is presented in Figure 2. The excitation spectrum consists of a broad peak in the range 316–421 nm. Superimposed on this peak are the peaks; 324 nm, 330 nm, 335 nm, 347 nm, 362 nm

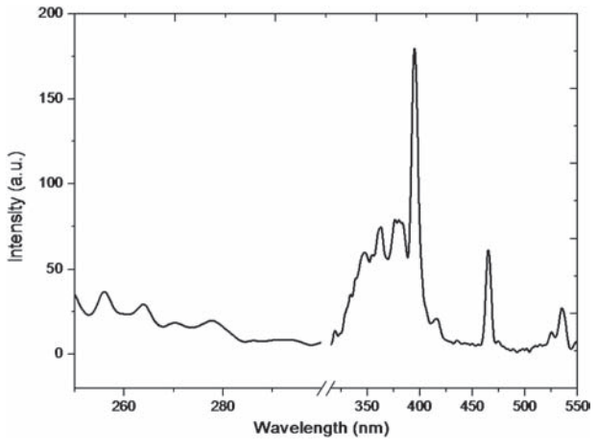

Fig. 2. Photoluminescence excitation spectra for ZnS:Eu^{3+}/MA nanophosphors.

($^7F_0 \rightarrow {}^5D_4$), 382 nm ($^7F_0 \rightarrow {}^5L_7$), 394 nm ($^7F_0 \rightarrow {}^5L_6$), and 418 nm ($^7F_0 \rightarrow {}^5D_3$). The other peaks are 465 nm ($^7F_0 \rightarrow {}^5D_2$), 524 nm ($^7F_0 \rightarrow {}^5D_1$) and 534 nm ($^7F_0 \rightarrow {}^5D_1$). The peaks at 320–347 nm are assigned to the band edge excitation of ZnS nanocrystals, since Eu^{3+} has negligible excitation cross-section at 347 nm.[20] These peaks are however very weak and leads to weak emissions of red light from Eu^{3+} at 614 nm ($^5D_0 \rightarrow {}^7F_2$), nevertheless, the presence of these bands in the excitation spectra strongly suggest energy transfer from the ZnS host to the Eu^{3+} ions.[21–23] The other lower energy peaks at 362–534 nm corresponds to the resonant excitation bands of Eu^{3+} ions.

The photoluminescence emission (PL) properties of ZE1 and ZE2 under 394 nm excitation wavelength are shown in Figure 3(A), while the PL of ZE5 under excitations at various wavelengths (289, 345, 365, 394 and 465 nm) were also investigated, and the results are shown in Figure 3(B). Consider the ZE5 sample excited under 289 and 345 nm. In addition to the observed broad emission peak at 437 nm, a weak emission peak at 614 nm associated to intra-configurational emission of Eu^{3+} ions was also observed. The broad peak at 437 nm is associated to sulfur vacancy[24] and the deconvolution of this peak yield defects related peaks at 423, 419, 446 and 467 nm with Eu^{3+} peak located at 614 nm. The defect related peaks at 419, 446, and 447 nm are close to the resonant values of Eu^{3+} ions and their presence shows that the energy transfer from ZnS to Eu^{3+} ions is from defects mediated.

Upon resonant excitation at 394 and 465 nm, the emission spectrum is dominated by the transitions; ($^5D_0 \rightarrow {}^7F_0$), ($^5D_0 \rightarrow {}^7F_1$), ($^5D_1 \rightarrow {}^7F_1$), ($^5D_1 \rightarrow {}^7F_2$), ($^5D_0 \rightarrow {}^7F_3$), and ($^5D_0 \rightarrow {}^7F_4$) associated with Eu^{3+} ions. The presence of the forbidden transitions ($^5D_0 \rightarrow {}^7F_0$) and the high intensity of the hypersensitive electric dipole transitions ($^5D_0 \rightarrow {}^7F_2$) and ($^5D_0 \rightarrow {}^7F_4$) indicate a low symmetry of the Eu^{3+} ions site. The low non-centrosymmetry (i.e., lattice distorted) site of Eu^{3+} is supported by the values of the intensity ratio[25] (i.e., $R_0 = (^5D_0 \rightarrow {}^7F_0)/(^5D_0 \rightarrow {}^7F_1)$). The R_0 values

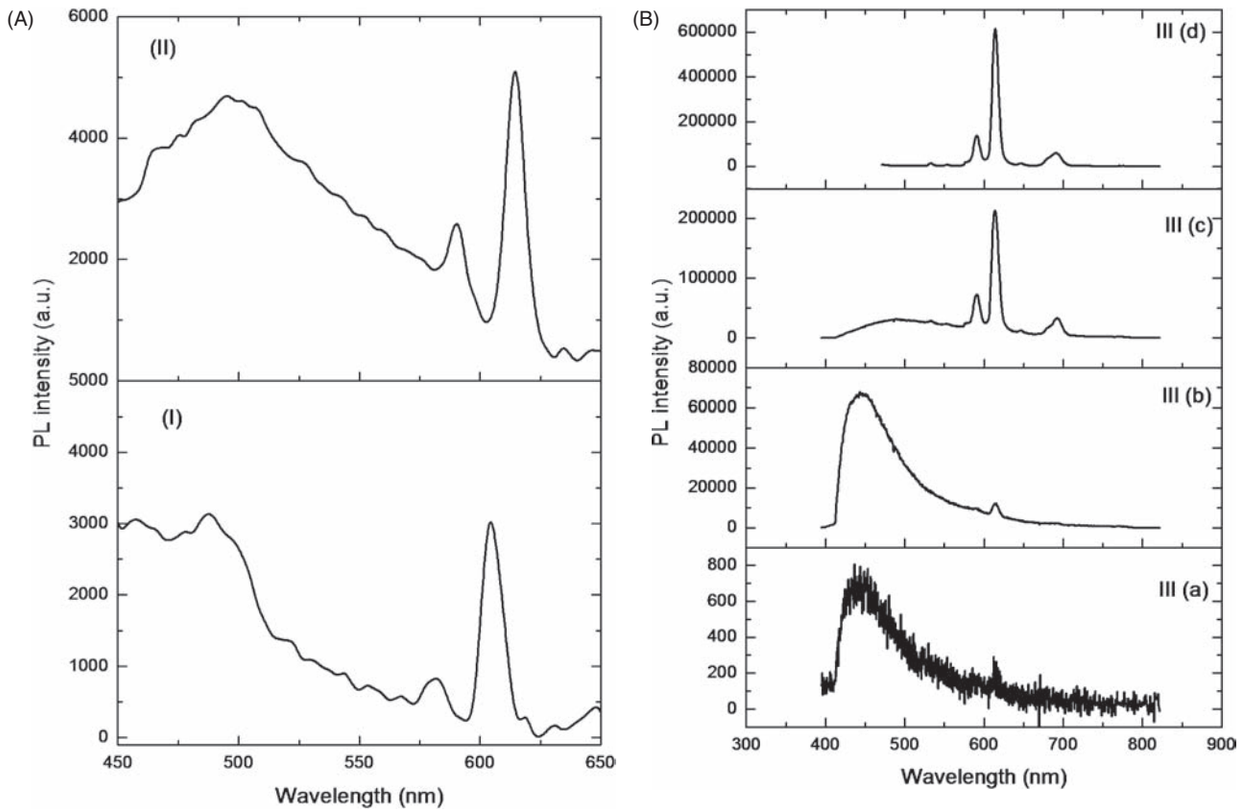

Fig. 3. (A) Photoluminescence emission spectra of (I) ZE1 at 394 nm, (II) ZE2 at 394 nm (B) Photoluminescence emission spectra of (III) ZE5: at (a) 289 nm, (b) 345 nm, (c) 394 nm and (d) 465 nm excitation wavelengths.

range from 1 to 4.4 and increased with increase in excitation wavelengths. The higher the intensity ratio the lower is the site symmetry which enables an enhancement in the red light emission of Eu^{3+} ions in the ZnS matrix.

The fact that there is variation in the red emission intensity ($^5D_0 \rightarrow {}^7F_2$) transition with changes in the excitation wavelengths show that the ZE5 sample is composed of different particles sizes which are located at different sites. Moreover, similar to the report by Georgescu et al.[26] Eu^{3+} in a site with higher asymmetry ratio ($R_o = 4.4$) may be located at a nanocrystal's surface while those with smaller R_o values may be positioned in the ZnS lattice.

Furthermore, it is clear from Figures 3(A) and (B) that the intensity of red light emission is dependent on the Eu^{3+} ions concentration. ZE5 sample is found to be the best red light emitter with the highest intensity.

3.3. SEM and TEM Analysis

Scanning electron micrographs (SEM) of the three samples ZE1, ZE2 and ZE5 nanoparticles (Figs. 4(a)–(c)) show that the particles are agglomerate with irregular size distribution. The surfaces of the nanoparticles are however smooth indicating that they are well passivated by the methacrylic acid. The elemental composition analysis using energy dispersive X-rays spectroscopy (EDS) shows the presence of zinc, sulfur and europium (Fig. 4(d)). The $[Zn^{2+}/S^{2-}]$ is about 2:1 indicating that the synthesized $ZnS:Eu^{3+}$ nanophosphors are sulfur deficient. The aluminium found in the EDS spectrum is probably from the aluminium grid and the carbon could be from the carbon tape used to hold the sample on the grid.

Transmission electron microscopy (TEM) images for ZE2 sample are also presented in Figure 5 for the purpose of comparison. In Figure 5(a) the images are spherical with average crystallite size of 4.33 nm. The discrepancy in the crystallite dimension from TEM and SEM images is due to the fact that SEM analysis often reveals the secondary particles which are usually agglomerates of the smaller (primary) particles while TEM analysis reveals the primary particles themselves[27] [Shrivastava et al. 2009]. Higher magnification TEM (HRTEM) images of individual crystallites were recorded in order to resolve the lattice planes. The d interplanar distance obtained from the HRTEM micrograph and shown in Figure 3(b) are similar to that for cubic ZnS polymorph.

3.4. Structural Studies

The X-ray diffraction patterns of all samples are shown in Figure 6. The three diffraction peaks in all the samples match well with those of the cubic ZnS reported in ICCD

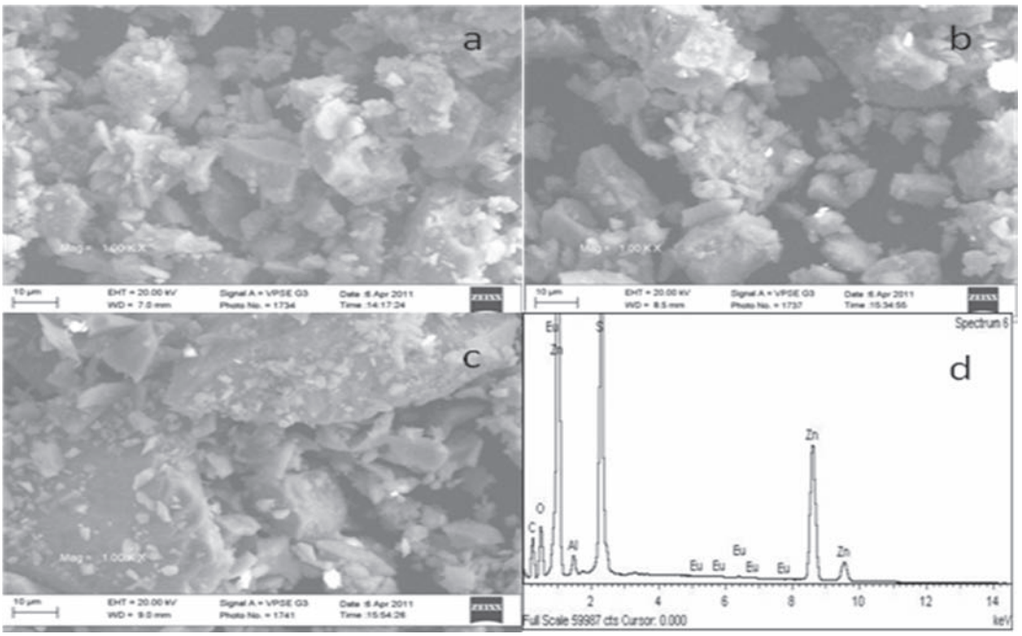

Fig. 4. SEM micrographs of (a) ZE1, (b) ZE2, (c) ZE5 and (d) EDX spectra of ZE5 sample.

powder diffraction file No. 00-01-0792. The three diffraction peaks at 2θ values of about 28.79, 48.14 and 57.31° correspond to (111), (220) and (311) planes respectively. No other impurity peaks such as Eu^{3+} ions were detected indicating the phase purity of the ZnS samples. The broad diffraction peaks indicate nanocrystallite size distribution of ZnS nanocrystal. The d-spacing as shown in Figure 4(b) is 3.17 Å and the value of the lattice constant, a, was calculated to be 5.491 Å. The mean crystalline sizes were calculated from the full-width at half-maximum (FWHM) of the three prominent peaks in the XRD pattern using the Debye Scherrer formula.

$$D = \frac{0.94\lambda}{\beta \cos\theta} \tag{5}$$

where, D is the crystallite size, λ is the wavelength of X-ray, β is the FWHM and θ is the Bragg's angle.

The result of crystallite sizes calculated from XRD patterns and the Schrrer's equation is also presented in Table I. From the result, the average crystallite sizes of the nanoparticles are in the strong quantum confinement regime.[14]

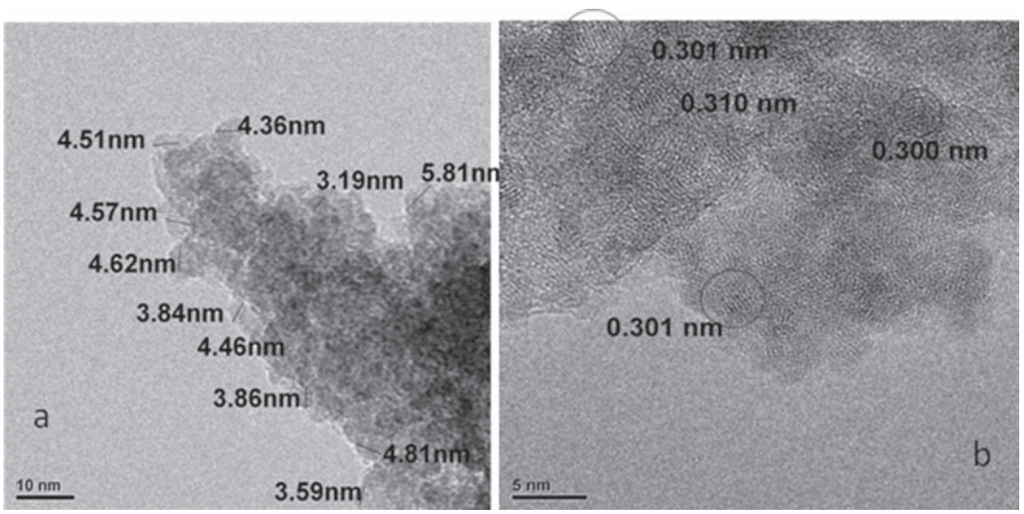

Fig. 5. TEM images (a) particles shapes and size distribution, (b) lattice parameters and fringes.

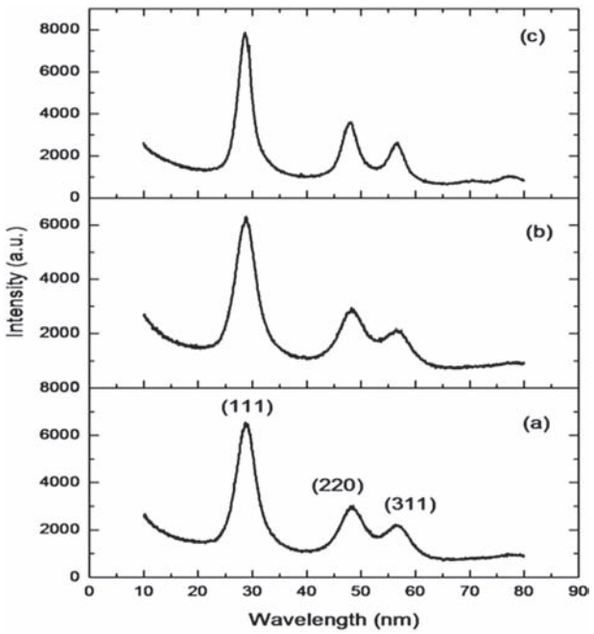

Fig. 6. XRD pattern of (a) ZE1, (b) ZE2 and (c) ZE5.

3.5. FTIR Studies

Fourier transform infrared spectral (FTIR) in Figure 7 confirms the presence of the capping agent and the acetate even after rigorous washing. The peak at 478 cm^{-1} is assigned to the metal—oxygen bonds (Eu—O).[28] while the peak at around 617 cm^{-1} originate from ZnS band, possibly due to Zn—S stretching.[29] Vibration mode peaks at 1172 and 1402 cm^{-1} are assigned to the C—O stretching band and in-plane bending respectively. The absorption bands at 1564 cm^{-1}, 1708 cm^{-1}, and 3182–3441 cm^{-1} are due to O—C—O asymmetric stretching, O—H stretching and C=O stretching bands respectively of the carboxylic acid.[29, 30] Hence, the existence of the above mentioned bands confirms the presence of ZnS and capping agent (α-Methacrylic acid, MA). The presence of MA after rigorous washing of the colloidal nanoparticles suggests that MA inhibits the growth of particle by steric stabilization. In ZnS:Eu, the passivation with MA would no doubt help to reduce surface trap site density. This would consequently reduce non-radiative recombination process, increasing thereby the luminescence.

Fig. 7. FTIR of $ZnS:Eu^{3+}$ capped with MA.

4. CONCLUSION

We have successfully synthesized Eu^{3+}-doped ZnS nanoparticles (quantum dots) whose dimensions are comparable to the exciton Bohr radius of ZnS. The synthesized nanoparticles exhibit quantum confinement effect evident from the enlarged bandgap evidence by a blue shift of the absorption spectrum and the broadening of the diffraction peaks. The intensity of red light emitted from the synthesized ZnS:Eu nanophospors is size and site dependent. There is clear evidence that energy transfer from the ZnS host to Eu^{3+}, though the emission intensity is weak.

Acknowledgment: The researchers wish to acknowledge some financial support (grant) by the National Agency for Science and Engineering Infrastructures Abuja, Nigeria (NASENI) to carry out part of this work. We also wish to thank Mr. Viana Bruno of Laboratoire de chemie de la matiere Curie Condense de Paris, France for the free photoluminescence characterization.

References and Notes

1. OIDA, Light Emitting Diodes (LEDs) for General Illumination: An OIDA Technology Roadmap. Sandia National Laboratory Pub., Washington DC **(2001)**.
2. E. F. Schubert, Light-Emitting Diodes, 4th edn., Reprint, University Press, Cambridge, UK.
3. E. F. Schubert and J. K. Kim, *Science* 308, 1274 **(2005)**.
4. D. Yeh, C. Huang, C. Lu Yang, and C. Yang, *SPIE Newsroom*, http://spie.org/documents/Newsroom/Imported/1069/1069-2008-02-28.pdf **(2008)**, pp. 1–3.
5. H. S. Yang, S. Santra, and P. H. Holloway, *J. Nano Sci. Nanotech.* 5, 1364 **(2005)**.
6. N. Shepherd and P. H. Holloway, Handbook on Electroluminescent Materials Part 1; II–IV Group Materials (Zinc Sulphide), IOP Publishing Ltd., Chap. 2.
7. W. Q. Peng, G. W. Cong, S. C. Qu, and Z. G. Wang, *Opt. Mater.* 29, 313 **(2006)**.
8. C. Xueyuan, L. Wenqin, L. Yongsheng, and L. Guokui, 25, 515 **(2007)**.
9. M. Banski and A. Podhorodecki, *Materials Science-Poland* 28, 1 **(2010)**,
10. A. A. Bol, J. Ferwerda, J. A. Bergwerff, and A. Meijerink, *J. Lumin.* 99, 325 **(2002)**.
11. K. Bennemans, *Chem. Rev.* 109, 4283 **(2009)**.
12. P. A. Jose, Lopez, Lopez, E. Cordoncillo, P. Escribano, F. Pelle, B. Viana, and C. Sanchez, *J. Mater. Chem.* 18, 5193 **(2008)**.
13. D. K. De, *J. Chemical Physics* 79, 535 **(1983)**.
14. http://cnx.org/content/m43554/latest/.
15. L. E. Brus, *J. Chem. Phys.* 80, 4403 **(1984)**.
16. J. Z. Zhang, *J. Phys. Chem B* 104, 7239 **(2000)**.

ARTICLE

17. J. M. Auxier, M. M. Morrell, R. B. West, S. Honkanen, A. Schulzgen, N. Peyghambarian, S. Sen, and N. F. Borrelli, *Appl. Phys. Lett.* 85, 6098 **(2004)**.

18. S. K. Kulkarni, S. Kalele, S. W. Gosavi, and J. Urban, *Current Science* 91, 1038 **(2006)**.

19. M. Sharma and S. O. P. Kumar, *Digest Journal of Nanomaterials and Biostructures* 3, 189 **(2008)**.

20. S. Sadhu, P. S. Chowdhury, and P. A. Patra, *J. Lumin.* 126, 387 **(2006)**.

21. A. A. Bol, R. van Beek, and A. Meijerink, *Chem. Mater*. 14, 1121 **(2002)**.

22. G. Ehrhart, B. Capoen, O. Robbe, F. Beclin, P. H. Boy, S. Turrell, and M. Bouazaoui, *Opt. Mater.* 30, 1595 **(2008)**.

23. D. Wang, G. Xing, M. Gao, L. Yang, J. Yang, and T. Wu, *The Journal of Physical Chemistry C* 115, 22729 **(2011)**.

24. S. K. Mehta, S. Kumar, S. Chaudhary, and K. K. Bhasin, *Nanoscale Res. Lett.* 4, 1197 **(2009)**.

25. M. Banski, A. Podhorodecki, and J. Misiewicz, *Materials Scince-Poland* 28, 218 **(2010)**.

26. S. Georgescu, A. M. Chinie, A. Stefan, and O. Toma, *Journal of Optoelectronics and Advanced Materials* 7, 2985 **(2005)**.

27. R. Shrivastev, M. Gupta, V. Sharma, J. Shrivastava, A. Solanki, A. Singh, V. R. Sat Sang, and S. Das, *Bull. Mater. Sci*. 32, 23 **(2009)**.

28. J. H. Jeong and H. Kyoung, *J. Phys. Chem. C* 908903 **(2009)**.

29. B. Staurt, Infrared Spectroscopy: Fundamentals and Applications, John Wiley & Sons, Ltd. (2004)

30. E. V. Brusau, J. C. Pedreggosa, G. E. Narda, E. P. Ayala, and E. A. Oliveira, *The Journal of Argentine Chemical Society* 92, 43 **(2004)**.

ARTICLE